Available online at www.sciencedirect.com
ScienceDirect
Cement and Concrete Research 37 (2007) 1483–1495
Cement and Concrete Research

# Phase composition gradient in leached polluted cement monoliths

Matteo Leoni [a,*], Paolo Scardi [a], Renato Pelosato [b], Isabella Natali Sora [b], Giovanni Dotelli [c], Paola Gallo Stampino [c], Arianna Lo Presti [d]

[a] Department of Materials Engineering and Industrial Technologies, University of Trento, Via Mesiano 77, 38050 Trento, Italy
[b] Department of Industrial Engineering, University of Bergamo, INSTM R.U.-Unibg, viale Marconi 5, 24044 Dalmine, Italy
[c] Department of Chemistry, Materials and Chemical Engineering 'G. Natta', INSTM R.U.-Politecnico di Milano, Piazza L. da Vinci 32, 20133 Milano, Italy
[d] Department of Earth Science 'Ardito Desio', University of Milano, via Mangiagalli 34, 20133 Milano, Italy

Received 18 July 2006; accepted 13 August 2007

**Abstract**

The long-term behaviour of cement monoliths containing an organic waste, was investigated by means of a 14-month dynamic-leach-testing in deionised water.

The degree of hydration and the phase composition were measured by Thermal Analysis (TGA/DTA), X-ray Powder Diffraction (XRD) and Energy Dispersive X-ray Spectroscopy (EDXS).

X-ray data, analysed by the Rietveld method, provided a detailed quantitative information on the in-depth crystalline phase distribution in the specimens. Crossed with TGA and spectroscopic data and supported by the results of kinetic/hydration calculations, the diffraction results provide a detailed description of the in-depth phase composition gradient in the leached monoliths.

In particular, 14-month old specimens show a clear leaching zone with predominance of CSH and calcite near the surface and low abundance of the other usual cement constituents. The material is not completely effective in retaining the contaminant.


*Keywords:* E. Waste management; B. X-ray diffraction; B. EDX; C. Long-term performance, D. Organic materials

## 1. Introduction

Cement-based stabilisation/solidification (S/S) is a well-established and widespread technology for the treatment of hazardous wastes (e.g. substances containing heavy metals or radioactive elements) before disposal or reuse [1–3]. Basically, the S/S technology involves the addition of a cementitious binder (e.g. Portland cement) to the waste (granular or liquid) to obtain a monolithic solid. This monolith is intrinsically porous [4], but it is structurally stable and possibly shows a good compressive strength [5]. Owing to this residual porosity, the surface area that can be potentially in contact with the leachant is larger than the simple external surface [6]. The leaching agent can change both the structure of the pores and the phase composition of the cement as it can enter the open porosity, contact the solidified waste and carry some contaminants out. For example, Bishop et al. [7] found that after a 90-day sequential leaching test the pore structure had markedly changed, primarily due to the dissolution of calcium hydroxide.

Not all reactions occurring during leaching are deleterious: the precipitation of $CaCO_3$ into the pores [8], for instance, can be beneficial as it strengthens the matrix and reduces its permeability; moreover, certain toxic species, such as zinc [8] or strontium [9], may precipitate forming calcium metal double carbonates, resulting in lower net leaching. However, Walton et al. [9] found an increase in apparent diffusion coefficient for unreactive species such as nitrates.

As a consequence of dissolution and/or precipitation reactions, in leached monolithic samples a sharp leaching boundary can be well identified [10–12]. A number of models have been developed to describe leaching from solidified wastes

* Corresponding author. Tel.: +39 0461 882416; fax: +39 0461 881977.
*E-mail address:* Matteo.Leoni@unitn.it (M. Leoni).

0008-8846/$ - see front matter © 2007 Elsevier Ltd. All rights reserved.
doi:10.1016/j.cemconres.2007.08.013

Table 1
Raw oxide composition and corresponding Bogue calculation for the OPC II AL 42,5 R

| | |
|---|---|
| *Raw oxide composition (wt.%)* | |
| CaO | 59.25 |
| $SiO_2$ | 17.9 |
| $Al_2O_3$ | 4.25 |
| $Fe_2O_3$ | 1.63 |
| $SO_3$ | 3.58 |
| $Na_2O$ | 4.23 |
| $K_2O$ | 2.04 |
| MgO | 1.68 |
| LOI (Loss on Ignition) | 6.28 |
| CaO free (free lime) | 2.21 |
| Insoluble residue | 0.16 |
| *Bogue calculation (wt.%)* | |
| $C_3S$ | 33.34 |
| $C_2S$ | 25.87 |
| $C_3A$ | 8.37 |
| $C_4AF$ | 4.96 |
| $CSH_2$ | 7.69 |
| $CaCO_3$ | 7.97 |
| $MgCO_3$ | 2.24 |

The amount of calcium and magnesium carbonates was estimated from the LOI properly corrected for water loss.

[13,14]. In the late 80s it was proposed to employ the S/S technology also for the immobilisation of organics, on condition that pre-adsorbents were used [15]. Among the categories of potential pre-adsorbent materials, organophilic clays seem to offer a valid cost-effective choice. However, the literature is scarce [16]; a few works can be found on the stabilisation/solidification of organic wastes into a cement matrix using organophilic clays as pre-adsorbents [15,17–22], and even fewer describe the leaching of solidified wasteforms containing organic materials [23,24]. On the overall, the results were promising; most works used model organic pollutants to test the effectiveness of S/S technology: phenols and chlorophenols [15,17,19,20], chloronaphtalene [17,20] and chloroaniline [22], while fewer used industrial wastes [15,18,21] with an organic load (TOC) ranging from 37 to 123 g/L [15], 15 g/L [18] and 320 g/L [21].

In this work 2-chloroaniline (2-CA), a member of the highly toxic family of aromatic amines, was chosen as a model pollutant and sorbed on an organic-pillared montmorillonite clay. The resulting waste was then converted into a solidified monolith by using ordinary Portland cement; the long-term stability of the so-obtained wasteforms was investigated using a combination of analytical techniques.

## 2. Experimental

### 2.1. Materials

Ordinary Portland Cement (OPC) Type II A-L 42,5R (UNI ENV 197) by Cementirossi s.r.l. (Italy) was used (Table 1); it is a calcareous cement with about 7.5 g of calcite per 100 g of dried sample.

A montmorillonite clay, pillared with a phenolic resin (organophilic) and supplied by Laviosa Chimica Mineraria s.r.l. (Italy) was chosen as pre-adsorbant. The organic matter (om) content, determined by Thermogravimetric Analysis (TGA), was 0.044 $kg_{om}/kg$. The total surface area was determined by the Brunauer, Emmet and Teller (BET) physisorption method. Measurements were carried out on a Micromeritics Tristar 3000 instrument on the nitrogen adsorption–desorption isotherms at 77 K. Samples were pre-cleaned by heating at 95° under vacuum for 12 h. Resulting area was 3.6 $m^2/g$. The basal interlayer spacing of the clay d(001), as determined by X-ray diffraction, was 1.51 nm.

2-chloroaniline (2-CA, CAS # 95-51-2) of >99.5% purity (GC) from a commercial source (Fluka AG) was used as model pollutant. 2-CA is a toxic [25] amber liquid with amine odour boiling at 209 °C (density at 20 °C is 1.21 $g/cm^3$).

Waters MilliQ® (deionised) water (conductivity max. 0.05 μS/cm) was used in this work.

### 2.2. Sample preparation

Three water solutions (sol) containing, respectively, 5000, 15,000 and 25,000 $ppm_w$ (wt/wt) of the 2-CA pollutant ($p$) were mixed with the organoclay (oc) into 50 mL vials and left on a rotating arm for 24 h to allow for the sorption. These concentrations are representative of a moderate polluted industrial effluent, as may be inferred from the analysis of literature data [15,18,21]; indeed, the present 2-CA concentration in the water solution corresponds to TOC levels in the 2800–14,100 mg/L range.

A total of eight slurries (s), containing a different $p/oc$ ratio, was therefore prepared. Each slurry was admixed with OPC powder (c) and hand stirred to obtain a fresh homogeneous clay/cement paste. Polyethylene cylindrical moulds (3.2 cm height and 2.2 cm diameter) were partially filled with the paste and carefully sealed with Parafilm®. Six contaminated sets (2 specimens each) and two uncontaminated specimens (the latter used as a reference) were prepared and cured in an air-conditioned room at 23±1 °C for 28 days (herein named 28-day specimens). The starting composition of the pastes is summarised in Table 2. Two series of specimens can be identified, differing in the oc content: the A series containing 3.2wt.% oc and the B series containing 6.2

Table 2
Composition of clay-cement pastes

| Specimen | Cement, $c$ (wt.%) | Water, $w$ (wt.%) | $w/c$ | Organoclay, oc (wt.%) | Pollutant, $p$ (wt.%) | $p/oc$ |
|---|---|---|---|---|---|---|
| Aref | 64.52 | 32.26 | 0.5 | 3.23 | 0.00 | 0 |
| A1 | 64.41 | 32.21 | 0.5 | 3.22 | 0.16 | 0.050 |
| A2 | 64.21 | 32.10 | 0.5 | 3.21 | 0.48 | 0.150 |
| A3 | 64.00 | 32.00 | 0.5 | 3.20 | 0.80 | 0.250 |
| Bref | 62.50 | 31.25 | 0.5 | 6.25 | 0.00 | 0 |
| B1 | 62.40 | 31.20 | 0.5 | 6.24 | 0.16 | 0.026 |
| B2 | 62.21 | 31.10 | 0.5 | 6.22 | 0.47 | 0.076 |
| B3 | 62.02 | 31.01 | 0.5 | 6.20 | 0.78 | 0.126 |

Table 3
Organic pollutants and wasteforms compositions reported in literature works where organophilic clays were used as pre-sorbent agent in S/S processes

| Waste | Pollutant/solid ($10^{-2}$ g/g) | Pollutant/total ($10^{-2}$ g/g) | Water/cement (g/g) | Organoclay/cement (g/g) |
|---|---|---|---|---|
| 3-Chlorophenol low [17] | 3.43 | 2.78 | 0.35 | 0.5 |
| 3-Chlorophenol high [17] | 17.15 | 13.9 | 0.35 | 0.5 |
| Chloronaphtalene low [17] | 4.34 | 3.52 | 0.35 | 0.5 |
| Chloronaphtalene high [17] | 21.68 | 17.58 | 0.35 | 0.5 |
| Phenol [19] | 0.082 | – | – | 0.2 |
| 2-Chlorophenol [19] | 0.082 | – | – | 0.2 |
| 2,4 Dichlorophenol [19] | 0.082 | – | – | 0.2 |
| 2-Chlorophenol [20] | 13 | 9 | 0.44 | 0.2 |

wt.% oc (nominal). The organophilic clay contents here adopted are somewhat lower than those reported in the literature (at least twice as much lower, Table 3). Consistently, the total amount of pollutant introduced in the wasteforms is quite low, see for comparison the ratio pollutant-to-solid of other authors (Table 3).

To assess the hydration degree of 28-day-old specimens, one for each series was demoulded after the curing and furnace-dried at 85 °C till its weight reached a stable value. In order to preserve the organic pollutant, to stop the hydration process, i.e. to remove the free water, nor solvent replacement (for instance acetone or methanol soaking) neither D-drying procedure could be used; so, the rather unusual choice of 85 °C as drying temperature was chosen as a compromise between the need for a temperature high enough to allow fast removal of the water present in the specimen, but sufficiently low to volatilize a negligible amount of the organic waste. It should be noted that ettringite which is an important crystalline component of hydrated Portland cement, can be destabilised at high temperature [26], producing an amorphous (or nearly so) product to X-ray powder diffraction (XRPD). The so-dried monoliths were crushed and a fraction of the material was ground in an agate mortar; the resulting powders were stored in a desiccator to be successively used for XRD and TGA measurements.

Simultaneously, the other six cured monoliths (one for each set of contaminated pastes), were demoulded as to be used for a 14-month dynamic leach test (DLT) in deionised water.

At the end of the test, the six specimens were extracted from the leaching solution and cut in two pieces along the cylinder height with a water-cooled diamond saw. One half was ground and then employed for XRD and TGA measurements aimed at obtaining phase composition data. The other half, after polishing without epoxy resin impregnation, was employed for the through-thickness XRD and EDXS phase analysis. None of these specimens was desiccated after DLT.

### 2.3. Dynamic leach test (DLT)

The dynamic leach test was carried out in compliance with the UNI 8798 norm [27] and therefore started after 28-day curing. Each solidified specimen was smoothed, cleaned and hung, completely immersed, in a 500 mL jar filled with 250 mL of deionised water kept at 24 °C without agitation. Water was periodically renewed according to the cited norm (once a day the first week, twice the second week, once a week up to the sixth week, then once a month) and progressive extractions were carried out up to 14 months.

Although the jar was closed with a screw cap, because of the presence of the headspace and the regular water renewals the atmospheric $CO_2$ dissolution in deionised water could not have been prevented.

The concentration of 2-CA in leachates was determined at each renewal; the operation was performed by extracting the pollutant from the leachates with isooctane, and determining its concentration by gas chromatography (GC). GC analyses were performed with a Carlo Erba Mega mod. 5100 instrument, equipped with on-column injector, flame ionisation detector and HP fused silica capillary column (0.32 mm internal diameter and 50 m length) coated with 5% phenylmethylsilicone rubber, 0.5 μm thickness. The temperature was linearly raised from 70 °C to 130 °C at 4 °C/min, then to 250 °C at 10 °C/min and finally kept constant for 5 min at 250 °C.

By using the GC technique, concentration measurements are done on the 2-CA molecule in the whole and not to the single constituent atomic species, thus reducing the possibility of getting erroneous results.

### 2.4. Thermogravimetric analysis

TGA and Differential Thermal Analysis (DTA) were conducted on a DTA-TG SEIKO 6300 instrument in nitrogen atmosphere on ca. 20 mg powder specimens. Scanning was done from room temperature to 900 °C with a 10 °C/min heating rate. As an example, Fig. 1 shows the typical DTA/TGA curve (A1 specimen). Two weight-loss parameters were obtained from the

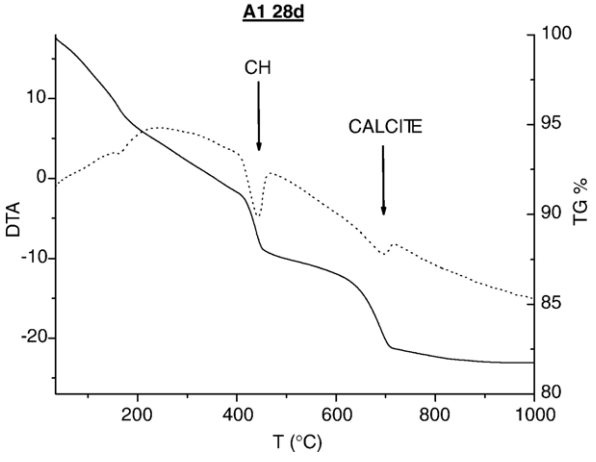


Fig. 1. DTA/TGA curves for the A1 specimen (28-day-old).

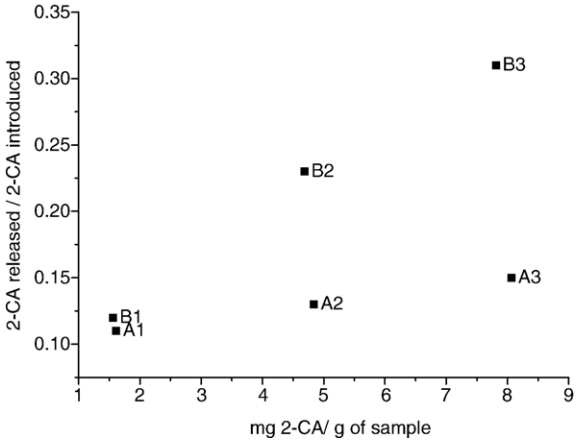


Fig. 2. Cumulative amount of 2-CA released ($p_{released}$, mg of 2-CA per gram of fresh sample) over the 2-CA initially introduced ($p_{introduced}$, mg of 2-CA per gram of fresh sample) in the samples after the 14-month DLT is reported *versus* the initial content of 2-CA, for specimens of the A and B series.

TGA curve: the stepwise loss associated with the calcium hydroxide, $Ca(OH)_2$, dehydration from about 400 to 500 °C, and the loss associated to calcite ($CaCO_3$), from 650 to 800 °C. All losses will be reported as grams per gram of dried sample (weight at 105 °C).

### 2.5. Mercury intrusion porosimetry (MIP)

The pore structure of the different systems was determined by means of mercury intrusion porosimetry (Pascal 440 porosimeter) for pressures up to 4000 bar ($r$= 0.2 nm according to Washburn model). The samples (fragments of 1.5–2.0 g) were previously oven-dried and then put in a dryer-vessel until the constant weight was reached.

### 2.6. X-ray powder diffraction

X-ray powder diffraction data were collected at room temperature on a Philips PW 1830 Bragg–Brentano diffractometer using graphite-monochromated Cu-Kα radiation (40 kV, 40 mA). A 2$\theta$ step of 0.02° and a measuring time of 12 s per step were chosen to obtain a sufficient signal/noise ratio.

Patterns for the through-thickness phase analysis were collected on a Philips X'Pert MRD 4-circle diffractometer on the cross-sectioned specimens. Copper radiation (40 kV, 30 mA) was used also in this case. A *quasi*-parallel-beam geometry was employed, obtained by means of a polycapillary collimator in the primary beam [28,29] and a flat crystal analyser (graphite) on the secondary arm. Beam size could be easily defined through a crossed-slits collimator.

Search match and qualitative phase analysis were done using the PANalytical X'Pert HighScore 1.0f software (© PANalytical B.V., Almelo, The Netherlands). Quantitative phase analysis was performed using the Rietveld method as implemented in the TOPAS 3.0 (Bruker AXS, Karlsruhe, Germany) software.

### 2.7. Environmental Scanning Electron Microscopy

Morphology observation and chemical analysis were conducted on the cross-sectioned specimens by means of a FEI XL30 Environmental Scanning Electron Microscope (ESEM) equipped with an Energy Dispersive X-ray Spectroscopy (EDXS) detector (EDAX FALCON) and operated at 20 kV/ 25 mA. The polished cross-sectioned specimens were analysed at 0.7 torr, without surface metallization. Elemental composition data were obtained from the X-ray spectroscopic signal collected over a large area of about 200 μm × 200 μm (taking into account the extension of the interaction volume plume) along the specimen radius.

## 3. Results and discussion

### 3.1. Leaching behaviour

There is no agreement in the literature concerning the optimal quantity of organoclay to be used in the S/S process: amounts of organoclay ranging from 3 to 20 g per 100 g of sample have been proposed so far [15–21]. In any case, a minimum quantity of organoclay is necessary to effectively sequestrate the contaminant [16]. In comparison with literature data [17,19,20] here it was used a much lower amount of organoclay with respect to the binder, 0.05 and 0.1 oc/c for A and B series, respectively; on

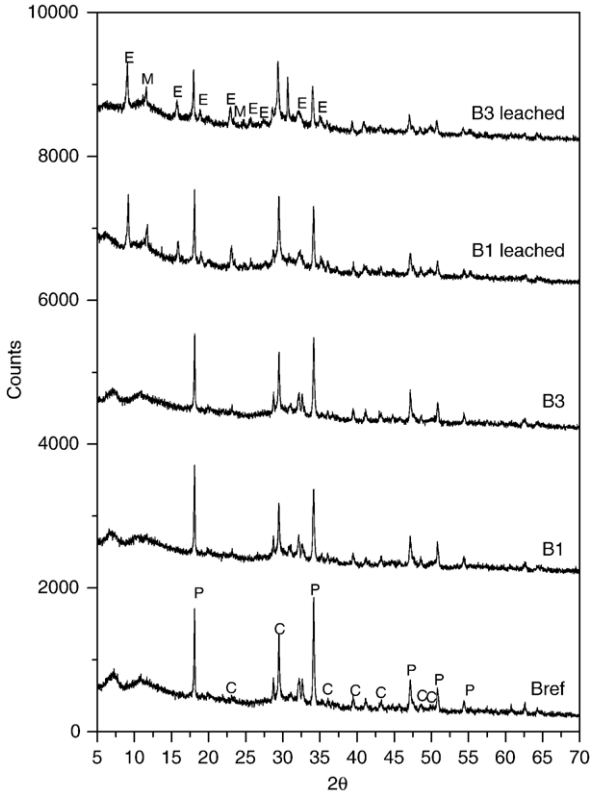


Fig. 3. XRD patterns of $B_{ref}$, B1 and B3 specimens after 28-day curing, and of B1 and B3 after 14 months of leaching. Only the 28-day-old samples were desiccated prior the measurement (E = ettringite, P = portlandite, C = calcite and M = monocarboaluminate).

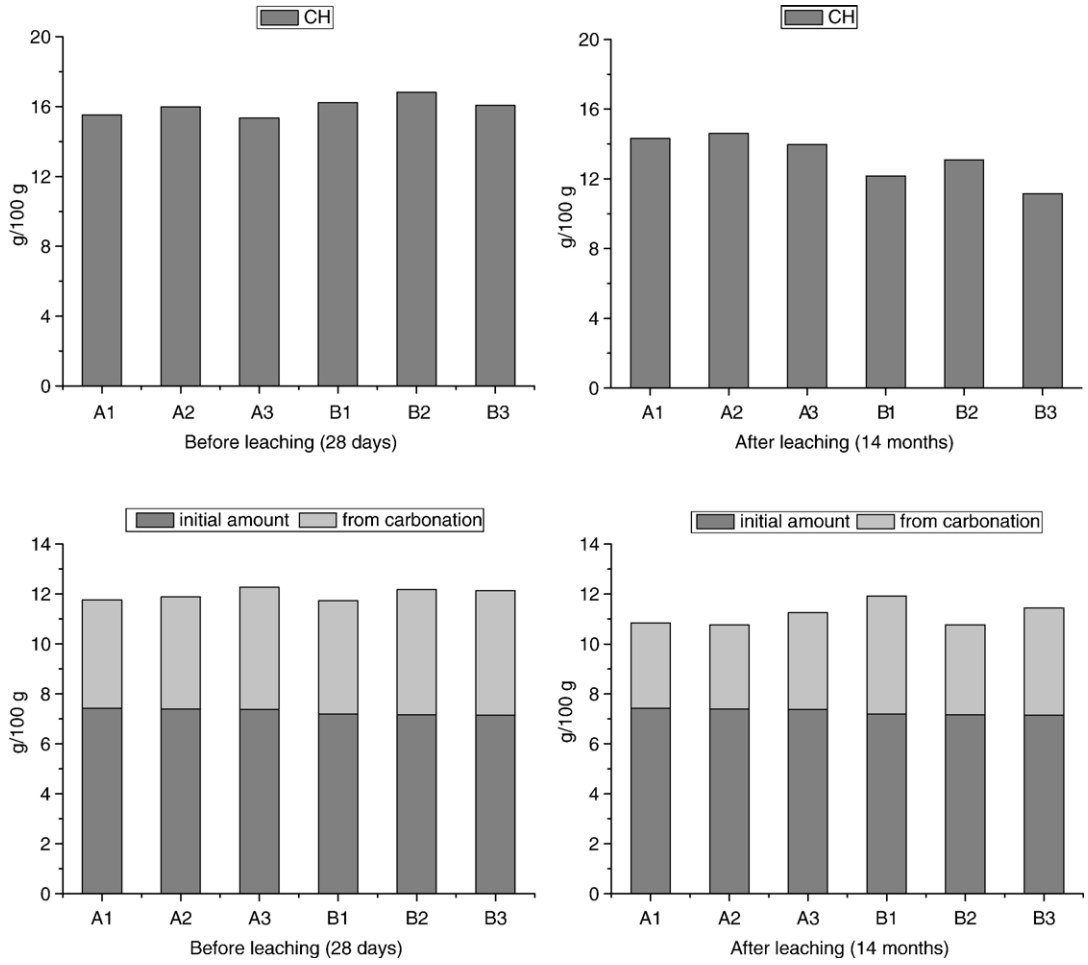


Fig. 4. Total amounts of portlandite and calcite determined by TGA for the 28-day-old and the leached specimens. All values are reported as g/100 g of dried sample.

average, other authors had inserted organoclay amounts ranging from 0.2 to 0.5 oc/c, Table 3.

In Fig. 2 the cumulative amount of 2-CA released ($p_{released}$, mg of 2-CA per gram of fresh sample) over the 2-CA initially introduced ($p_{introduced}$, mg of 2-CA per gram of fresh sample) in the samples after the 14-months DLT is reported *versus* the initial content of 2-CA, $p_{introduced}$.

While samples A1 and B1 have the same leaching behaviour (about 11 and 12% of $p_{released}$ with respect to $p_{introduced}$, respectively), sample B3 releases twice as much an amount of 2-CA than A3 (about 15 and 31% of $p_{released}$ with respect to $p_{introduced}$, respectively), and A2 and B2 lie in-between (about 13 and 23% of $p_{released}$ with respect to $p_{introduced}$, respectively).

From the DLT results it appears that the larger the amount of organoclay the worse the immobilisation of 2-CA; indeed, the B series samples contain twice as much organoclay than those of the A series (Table 2).

A reduction in the active organophilic area when going from low to high organoclay content (3.2 and 6.2 g/100 g in series A and B, respectively) might explain this striking leaching behaviour. Indeed, when the amount of organoclay is low, the size of the clay aggregates is small and the pollutant can be adsorbed on most of the available active area (surface and interlayer): by increasing the quantity of organoclay, the chance of agglomeration increases and so does the fraction of trapped organophilic sites; as a consequence, the concentration of available adsorption sites probably decreases.

The sorption mechanism of 2-CA onto organophilic clays has been demonstrated to be mainly physical in nature and due to the interactions between the 2-CA and the organic matter dispersed in the clay, which creates a favourable organophilic microenvironment [30]. Probably, the only direct interactions, if any, between the pollutant and the siliceous surface of the clay can just stem from a very weak hydrogen bonding, considering the slight basic behaviour of 2-CA. However, being absent any strong chemical binding between 2-CA and the organoclay the sorption process is partially reversible [30]; as a consequence, the pore solution inside the cement matrix can extract the pollutant from the organoclay which can leach out of the monolith in the presence of open porosity.

To confirm this hypothesis MIP analyses of all samples were carried out: the open porosity of A1, A2 and A3 specimens is 24.74, 25.99 and 27.58%, respectively, while that of B1, B2 and B3 is 29.57, 32.34 and 32.81%, respectively; there is no substantial difference in the average pore radius between the two series.

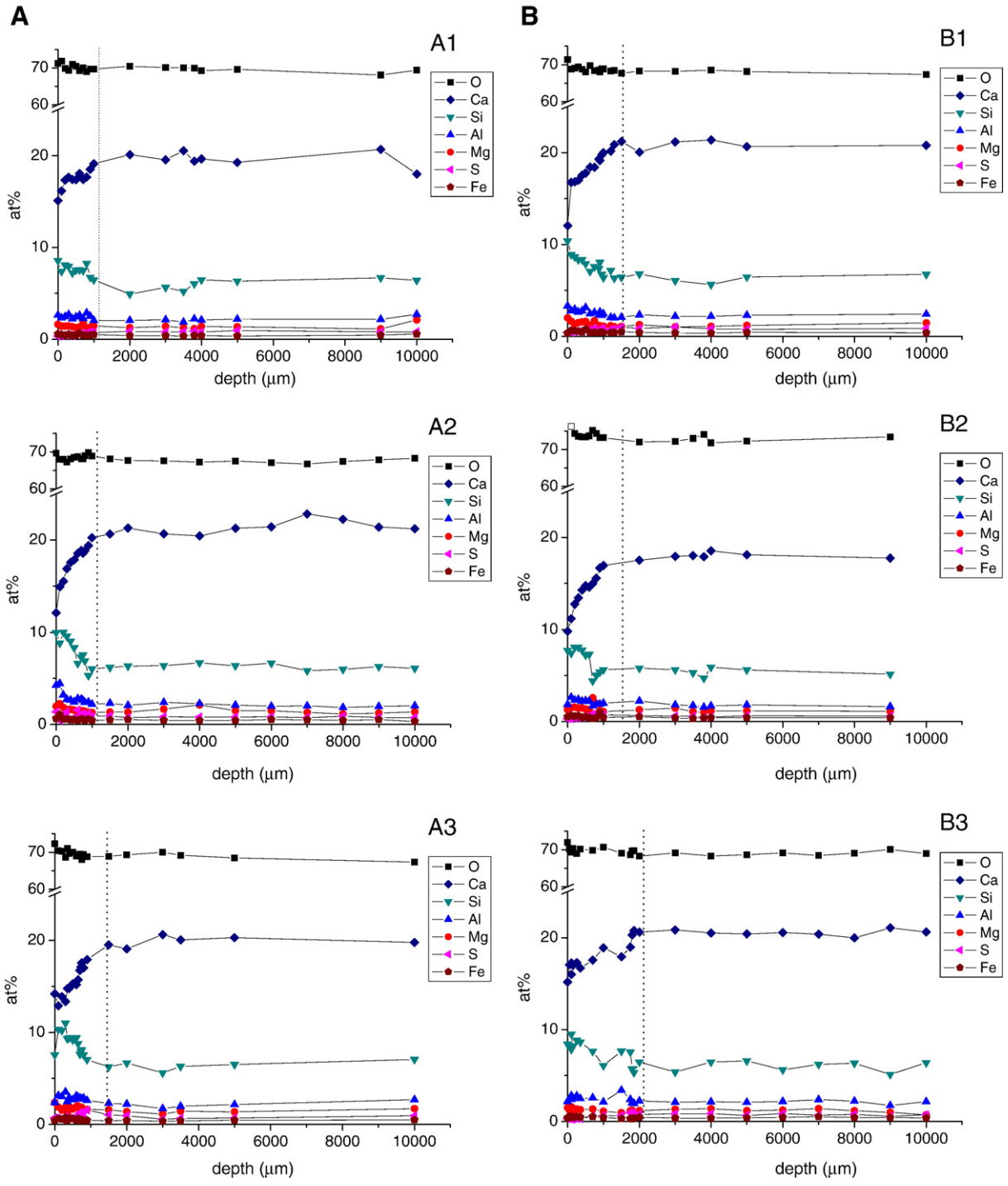


Fig. 5. Depth-resolved elemental composition profile (EDXS data) for the A (A) and B (B) series.

The addition of the organoclay seems to influence the total porosity, which is larger in the B series, but it does not alter sensibly the average pore radius, usually found in the 3–100 nm range [31] for mature cement pastes. The average pore radius values here found are in the 50–70 nm range, suggesting that there is a predominance of large and medium capillary pores: about 60% of the relative volume porosity is in the 100–10 nm pore radius range, and this kind of pores is well-known to have a substantial influence on the permeability [32]. Moreover, the organoclay amount influences the total specific surface area: 37 $m^2$/g in the B series samples which contain twice as much organoclay with respect to the A series samples, 25 $m^2$/g.

So the apparently counterintuitive worse leaching behaviour of B series samples seems to be reasonably accounted for by the monolith pore structure; it is well-known that relatively large pores, as those here found, have an adverse effect on permeability. Furthermore, the fraction of 2-CA released increases with its initial amount (from 0.11 to 0.15 and from 0.12 to 0.31 for series

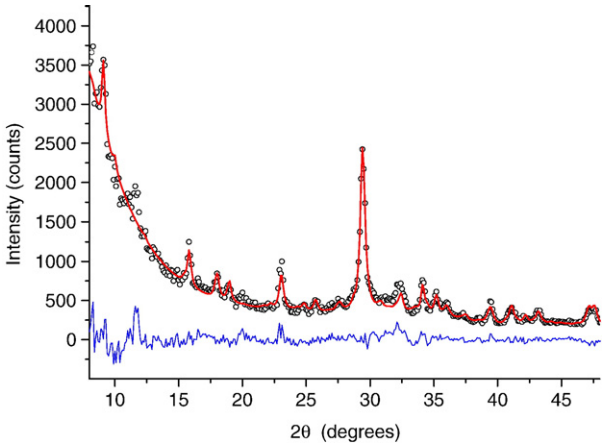


Fig. 6. Pattern of the B1 specimen collected at 0.75 mm from the surface: raw data (points), Rietveld modelling result (line) and residual (difference curve, below) are shown.

A and B, respectively) and the trend in porosity is exactly the same.

### 3.2. Average phase composition prior and after long-term leaching

Even at the highest concentration of 2-CA, i.e. 25,000 $ppm_w$, the same mineralogical phases are present in all 28-day-old specimens, i.e. tricalcium silicate ($C_3S$, $Ca_3SiO_5$ ICDD PDF-2 card 49-0442), β-dicalcium silicate ($C_2S$, $Ca_2SiO_4$ ICDD PDF-2 card 33-0302), calcium hydroxide (portlandite, $Ca(OH)_2$ ICDD PDF-2 card 44-1481), carbonates (calcite, $CaCO_3$ ICDD PDF-2 card 05-0586 and ankerite, $CaMg_{0.3}Fe_{0.7}(CO_3)_2$ ICDD PDF-2 card 41-0586) and amorphous calcium silicate hydrate (C-S-H). Data are in agreement with literature findings [30,33–36]. In Fig. 3 the X-ray diffraction patterns for specimens of the B1 and B3 sets are shown as an example, compared with those of a reference (28-day-old containing no organoclay). Overall phase composition and absolute amount of hydration products are not substantially altered by the organoclay.

Dynamic leaching tests were performed not only to assess the effectiveness of the S/S technology, but also to investigate the short and long-term physicochemical reactions that occurred in the solidified wasteforms [14]. In fact, the actual performance and long-term environmental impacts cannot be determined by leach tests alone which do not provide information on the physical (i.e. pore structure [37]) and chemical [38] changes occurring in the S/S wasteforms. To this purpose, the understanding of the leaching mechanisms is of paramount importance and requires the detection of the mineral transformations and the monitoring of common hydration products dissolution. In the 14-month leached pastes two additional phases were detected: ettringite ($Ca_6Al_2(SO_4)_3(OH)_{12}26H_2O$, ICDD PDF-2 card 41-1451) and monocarboaluminate hydrate ($Ca_4Al_2O_6CO_311H_2O$, ICDD PDF-2 card 41-0219). The presence of these phases is evident in Fig. 3 where the XRD patterns of specimens after DLT are compared with analogous ones measured at 28 days. Ettringite was not detected in any of the 28-day-old samples, probably because of the chosen drying treatment performed on these pastes to stop the hydration reactions [26].

Fig. 4 shows the variation of the average content of portlandite and calcite in all contaminated samples (28-day-old and after leaching) as obtained from the thermal analysis. All 28-day-old samples have a similar content of portlandite and calcite, i.e. about 16 and 12 g/100 g of dried sample, respectively.

In the first 28 days the hydration process in A and B series does not seem to be retarded by the presence of the contaminant; indeed, the portlandite content in control sample Aref, which is not reported in Fig. 4, is just a little larger than in contaminated samples A1, A2, A3 (17.6±0.9 *versus* 15.5±0.8, 16.0±0.8 and 15.4±0.8 g/100 g of dried sample, respectively); among Bref, B1, B2 and B3 there is no difference within the experimental error (16.2±0.8, 16.2±0.8, 16.8±0.8 and 16.1±0.8 g/100 g of dried sample, respectively). So the retarding effect observed in hydrating cement pastes directly admixed with 2-CA [33] is likely to be counterbalanced by the accelerating effect on the hydration of $C_2S$ and $C_3S$ due to the addition of clay minerals to OPC pastes [34].

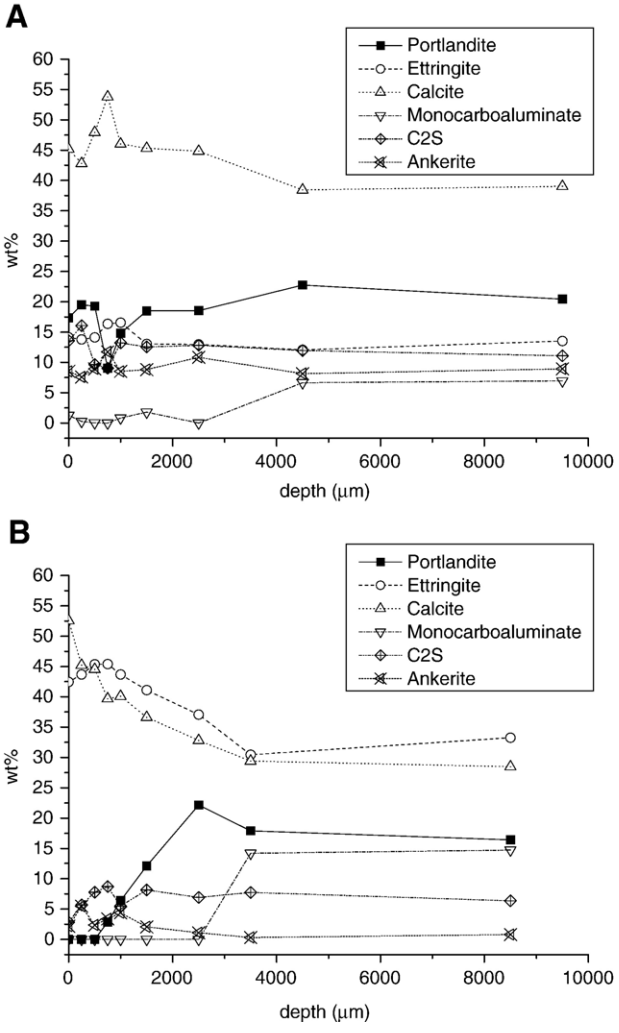


Fig. 7. Depth-resolved crystalline phase composition profiles for the A1 (A) and B1 (B) specimens as obtained from the Rietveld refinement.

Table 4
Model composition of 14 months leached samples in g per 100 g of fresh paste

| Phase | Names | A1 | A2 | A3 | B1 | B2 | B3 |
|---|---|---|---|---|---|---|---|
| $C_{1.7}SH_4$ | Amorphous CSH | 34.87 | 34.77 | 34.65 | 33.79 | 33.68 | 33.58 |
| $C_4AC\underline{C}H_{11}$ | Monocarboaluminate | 9.61 | 9.58 | 9.55 | 9.31 | 9.29 | 9.26 |
| $C_6A\$_3H_{32}$ | Ettringite | 12.04 | 12.01 | 11.97 | 11.67 | 11.63 | 11.60 |
| CH | Portlandite | 12.26 | 12.23 | 12.19 | 11.88 | 11.84 | 11.81 |
| Carbonates | Calcite and ankerite | 9.60 | 9.54 | 9.96 | 10.55 | 9.54 | 10.13 |
| $FH_3$ | Amorphous phase | 2.11 | 2.11 | 2.10 | 2.05 | 2.04 | 2.04 |
| Organoclay | | 3.50 | 3.49 | 3.48 | 6.76 | 6.74 | 6.72 |
| $C_3S$ | Tricalcium silicate | 0.00 | 0.00 | 0.00 | 0.00 | 0.00 | 0.00 |
| $C_2S$ | Dicalcium silicate | 6.45 | 6.43 | 6.41 | 6.25 | 6.23 | 6.21 |
| $C_3A$ | Tricalcium aluminate | 0.00 | 0.00 | 0.00 | 0.00 | 0.00 | 0.00 |
| $C_4AF$ | Calcium aluminum ferrite | 0.00 | 0.00 | 0.00 | 0.00 | 0.00 | 0.00 |
| $C\$H_2$ | Gypsum | 0.00 | 0.00 | 0.00 | 0.00 | 0.00 | 0.00 |
| $Na_2O$,$K_2O$ etc | Oxides | 4.04 | 4.03 | 4.01 | 4.96 | 4.94 | 4.93 |
| Residual H | Residual water | 5.52 | 5.81 | 5.68 | 2.78 | 4.07 | 3.72 |

The residual H is just the free water calculated as the difference between the initial amount of water and the bound water estimated by model calculation.

In the 14-month-old specimens, portlandite is somewhat decreased. This can be explained as an effect of both carbonation and dissolution [33–35,37,39], the latter due to calcium leaching occurring when the interstitial pore solution has a calcium concentration lower than the equilibrium one. The decrease is smaller in specimens containing less organoclay (ca. 15% in the A series against ca. 25% in the B series) and seems not influenced by the contaminant.

Most calcite is already present in the cement powder (about 7.5 g/100 g of dried sample); in the 28-day curing, before starting the DLT, there is an additional carbonation of all contaminated samples (about 12 g/100 g of dried sample), while during the DLT the calcite amount changes only slightly. Apparently, the DLT would not affect the amount of calcite, which varies only slightly in accordance with the TGA data; however, it is more likely that portlandite is being converted to calcite, which in turn reacts with AFm or AFt phases to produce carboaluminate species, as it will be better explained in the next sections.

### 3.3. Morphology and elemental and crystalline phase composition gradient in leached specimens

From a qualitative point of view, the cross-sections of all specimens show the same morphology under the ESEM. The monoliths are highly (macro) porous, but compact. In the leached specimens, a large fraction of the pores contains ettringite needles [37].

The phase contrast obtained by using the backscattered electrons was not sufficient to clearly identify the leaching zone boundary, otherwise evident to the naked eye.

A relative estimate of the in-depth elemental distribution was obtained for all specimens by EDXS. The spatial resolution of this technique is quite high (determined by the extension of the interaction region between electron beam and specimen), but information is only of chemical (elemental) nature. Only the elements showing a clearly detectable signal, i.e. carbon, oxygen, calcium, silicon, aluminium, magnesium, sulphur and iron, were investigated.

Fig. 5 shows the EDXS data for all the leached specimens. A clear compositional gradient is present in the near-surface region delimited by the leaching boundary (the depth at which the composition starts being constant), the latter indicated by a dotted line. In all investigated monoliths, leaching just of calcium up to a depth of about 2 mm is observed (Fig. 5).

X-ray diffraction is one of the most versatile techniques allowing for a quantitative determination of phase composition gradients. A high spatial resolution can be achieved by using a narrow beam size, whereas quantitative data can be obtained by processing the entire diffraction pattern using the Rietveld method [40]. Prerequisite to this, is the accurate identification of the crystalline phases present [41–43]. In fact, in the Rietveld method, physical data relative to the instrument (e.g. geometry, optical components and their dimensions) and structural information on the phases present (e.g. lattice and atomic positions data, crystallographic texture, presence of defects) are used to synthesise a pattern relative to the area bathed by the X-rays. Model parameters are adjusted within a Nonlinear Least SQuares (NLSQ) minimisation routine to match the experimental data. A quantitative phase composition can be obtained from the relative scale factors of the phases used in the modelling [40–43]. The result, however, is always of relative nature: phase composition values refer to the total crystalline fraction modelled by the Rietveld algorithm. Amorphous contribution, if any, is not automatically considered and additional information is thus needed to quantify it with respect to the crystalline phase [36]. Results from other measurement techniques or from the modelling of the hydration/leaching reactions can be used to recover the missing data.

Table 5
Model phase composition values (%) referred to the total crystalline fraction, including only the phases modelled by the Rietveld algorithm

| | $C_4AC\underline{C}H_{11}$ | $C_6A\$_3H_{32}$ | CH | Carbonates | $C_2S$ |
|---|---|---|---|---|---|
| A1 model | 19.97 | 25.02 | 21.65 | 19.95 | 13.4 |
| A1 Rietveld | 6.94 | 13.52 | 20.45 | 48.45 | 11.1 |
| B1 model | 19.81 | 24.82 | 19.62 | 22.45 | 13.32 |
| B1 Rietveld | 14.73 | 33.27 | 16.41 | 29.25 | 6.34 |

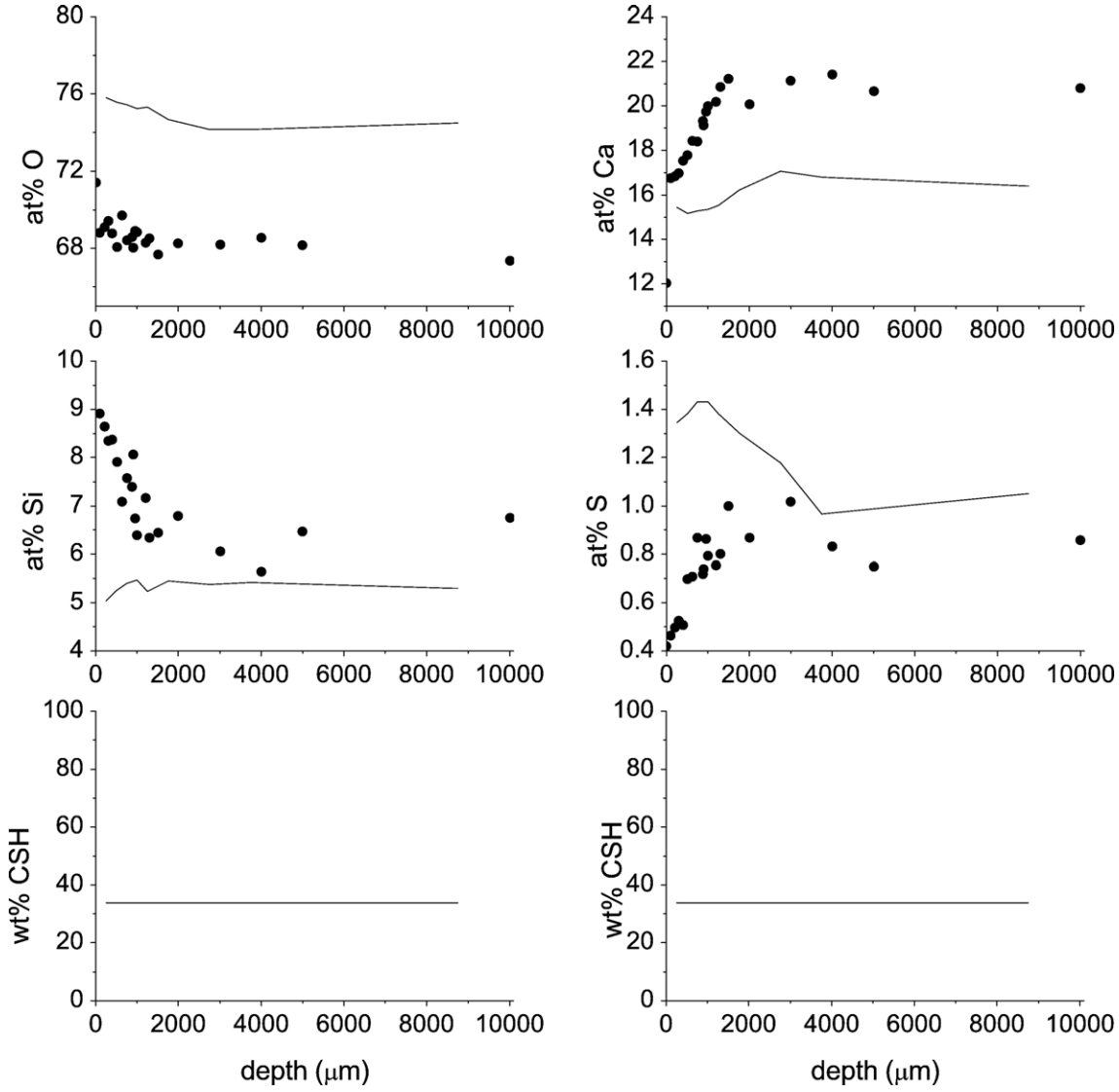


Fig. 8. B1 specimen: comparison between EDXS (dots) and raw Rietveld data (line).

In order to collect data at increasing depth, the cross-section (cut) of each specimen was thoroughly scanned along the specimen's radial direction: points along the whole diameter were collected, but only those relative to the radius will be presented, as the composition shows symmetry with respect to the axis of the monolith. At least 10 points were collected for each specimen along the radius: as a nonlinear phase composition gradient was expected, an uneven spatial sampling was adopted, collecting closer data points near the surface and widening the spacing at higher depths (cf. ESEM data).

Measurements were conducted using a 6 mm (width) by 0.2 mm (height) X-ray beam: the longer side of the beam footprint was laid along the longer dimension (height) of the cut specimen as to collect data on a ca. 0.25 mm wide strips at each depth step. The actual width of the measured strip is higher than the beam size due to the imperfect parallelism of the beam (divergence ~0.3°), imperfect parallelism of specimen edges and possible slight misalignment of the specimen (specimen tilt/rotation with respect to the beam).

Each pattern was processed with the PANalytical X'Pert HighScore© software to identify the crystalline phases, and subsequently with the Bruker TOPAS© Rietveld refinement software to obtain the quantitative information.

Fig. 6 shows one of the patterns refined by TOPAS: the agreement between data and model is remarkable, considering the quality of the data. Fig. 7 shows the result of the Rietveld refinement applied to the whole datasets for specimens A1 and B1 (results for the other specimens have been omitted for brevity): a through-thickness crystalline phase composition gradient is present. The extension of the near-surface leaching zone is compatible with that obtained by EDXS (cf. Fig. 5).

An increase in the width of the leach-affected zone has been observed for increasing percentage of pollutant in the starting paste. The long stay in deionised water changed the composition of the monoliths' near-surface which appears rich in carbonates and poor both in hydroxides and silicates with respect to the interior. In accordance with TGA results (cf. Fig. 4), a significant fraction of portlandite is still present in all specimens.

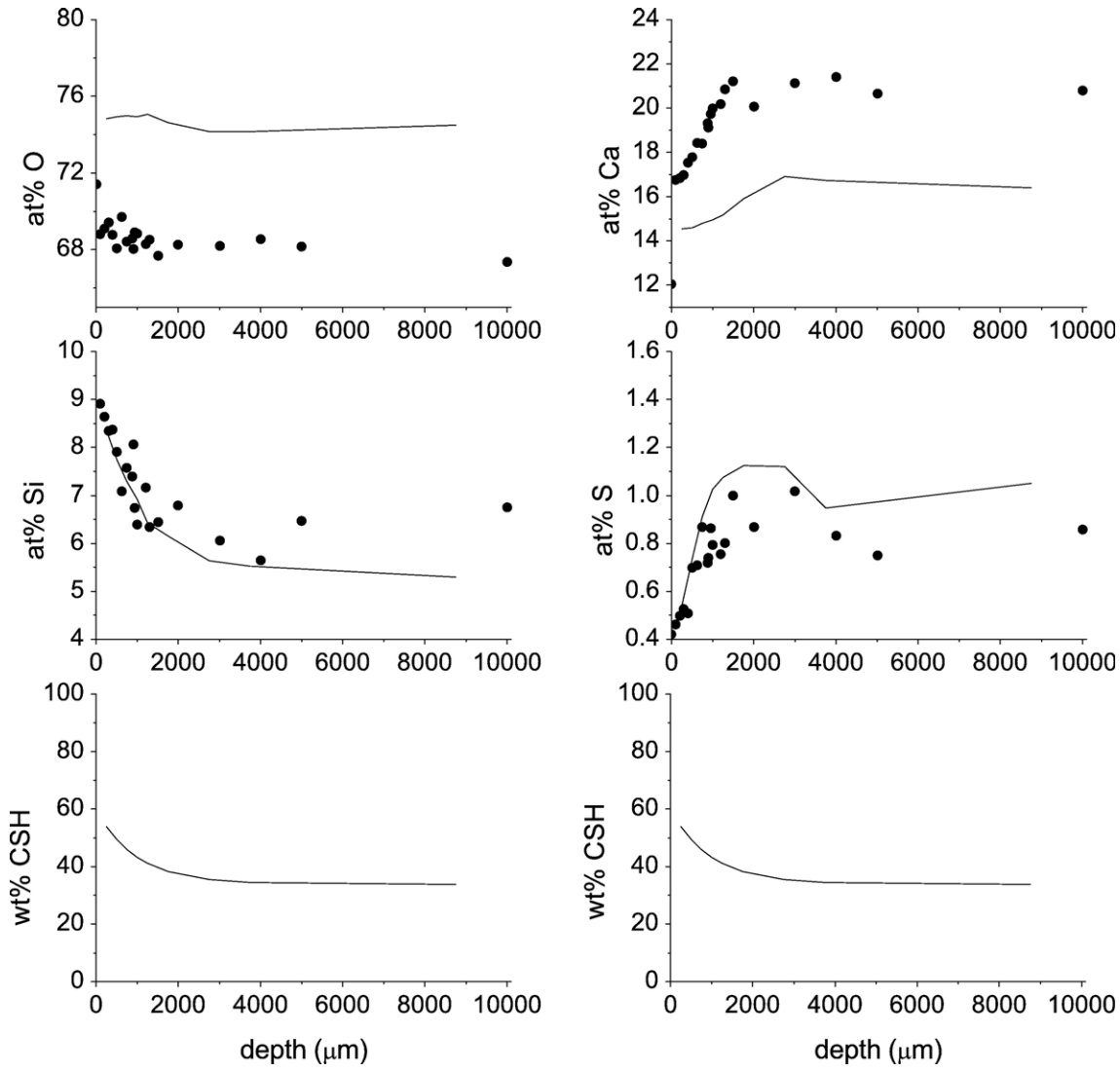


Fig. 9. B1 specimen: match between EDXS (dots) and Rietveld data (line) taking amorphous phase and its gradient into account.

The amount of ettringite, increasing towards the surface, and the fraction of $C_2S$ still unreacted after 14 months are unusually high.

It must be stressed again that the X-ray quantitative data proposed so far refer to the sole crystalline phases present in the specimen and therefore are not representative of the absolute phase distribution in the specimens, as the amorphous contribution is not included.

## 4. Determining the true phase composition gradient

As the EDXS and XRD data refer to the same specimens and are collected approximately in the same regions, they should be compatible. The expected difference is due to the presence of the amorphous C-S-H, measured by EDXS and not included in the Rietveld processing.

Two are the unknowns relative to the C-S-H: composition and percentage. The composition is influenced by several factors but the values are more or less uniform in the literature: an average $C_{1.7}SH_4$ composition is adopted here [36,44]. The percentage of amorphous present can be calculated in advance by using the kinetic models available in the literature. In order to do so, a kinetic calculation was done using the hydration reaction scheme suggested by Bentz [44] in order to estimate the phase composition of the contaminated pastes after 14 months of leaching. In the core of the specimens (where the leachant should have had zero or minor effects) the modelling results should be compatible with both EDXS and XRD Rietveld analyses. Starting from the Bogue composition data for the present cement (cf. Table 1), the calculation matched the following reaction scheme:

$$C_3S + 5.3H \Rightarrow C_{1.7}SH_4 + 1.3CH \quad (1)$$

$$C_2S + 4.3H \Rightarrow C_{1.7}SH_4 + 0.3CH \quad (2)$$

$$C_3A + 3C\$H_2 + 26H \Rightarrow C_6A\$_3H_{32} \quad (3)$$

where, as said before, $C_{1.7}SH_4$ is the gel-like C-S-H phase, $C\$H_2$ is gypsum and $C_6A\$_3H_{32}$ is ettringite, belonging to the group of AFt phases. In fact, after an initial rapid dissolution of $C_3A$, it is

generally observed an almost immediate precipitation of an amorphous calcium aluminate hydrate gel followed by the nucleation of crystalline products which can be AFm or AFt phases depending on the particular circumstances [45]. Usually the crystalline phase produced in the initial hydration stage is ettringite which becomes unstable when the liquid phase starts to be deficient in $Ca^{2+}$ and $SO_4^{2-}$ ions; as a consequence, there is a renewed hydration of $C_3A$ to form AFm phases (typically monosulphocalciumaluminate hydrate $C_4A\$H_{12}$) and this is also the usual reaction sequence adopted in highly sophisticated cement hydration simulation programs [44]. On the other hand, simplified hydration models discard ettringite formation and consider just AFm phases as final products [46,47].

However, part (or most) of the ettringite observed in the present samples after leaching is a secondary mineral (delayed ettringite) formed as a result of dissolution [37]. The leached specimens were in fact kept in water, where an amount of $CO_2$ is dissolved roughly corresponding to the atmospheric equilibrium concentration. In the presence of $CO_2$ the monosulphate is unstable and tends to exchange the sulphate ions with carbonate ones (transforming the monosulphate $C_4A\$H_{12}$ into monocarboaluminate $C_4A\underline{C}H_{11}$). The process is active already at room temperature when the local pH > 12 [48]; yet, in cement pastes containing more than about 0.5% $CO_2$, as in the present case, the conversion of ettringite into monosulphate is prevented and monosulphate is replaced by hemicarbonate or monocarbonate [49]. This causes an enrichment of the solution in sulphate ions that can promote the formation of the delayed ettringite. An alternative mechanism of late ettringite formation was suggested by Fu et al. [39]; in any case, the sulphate ions eventually end up in AFm or AFt phases.

With respect to the usual hydration scheme, two additional reactions were considered to account for the free lime hydration (reaction supposed to be instantaneous) and the presence of monocarboaluminate ($C_4A\underline{C}H_{11}$):

$$C + H \Rightarrow CH \tag{4}$$

$$3C_3A + 3C\$H_2 + 2C\underline{C} + 48H \Rightarrow C_6A\$_3H_{32} + 2C_4A\underline{C}H_{11} \tag{5}$$

Because the chosen cement is highly carbonatic (CEM II A-L 42,5R) and it is kept in water, an environment rich in $CO_2$ [49], reaction (5) was selected to describe delayed ettringite formation, following the approach adopted by Bentz [50] in the most recent version of the software CEMHYD3D to account for cement hydration in the presence of limestone. Under these conditions, the monocarboaluminate and the hemicarbonate form instead of the monosulphate by exchange of the sulphate and carbonate ions in the monosulphate favoured by the locally high carbonate concentration [51]. Last, the hydration sequence for the ferrite phase is the same as for $C_3A$: iron-substituted AFt or AFm phases form, together with an amorphous aluminium-substituted $Fe(OH)_3$ [45,52]. Under the simplified hypothesis that $C_4AF$ hydration products are just the same as those of $C_3A$, i.e. iron substitution is completely discarded, in cement hydration models [44,46,50] iron hydroxide is the phase normally used to account for iron mass balance. Being amorphous in nature, this phase is not revealed by XRD analysis; moreover, its content is almost negligible because of the low amount of iron in common Portland cements.

As far as calcite is concerned, no net variation is observed during DLT (Fig. 4), due to the balance between carbonation and consumption in monocarbonate formation (5) in the present reaction scheme the usual carbonation reactions [9] were discarded.

Using the given reaction scheme, the composition of all samples after complete hydration ("infinite time") was quantified. This information can be employed within a set of Avrami-type equations [46] in order to approximate the degree of hydration for each sample at 14 months. The general form of the Avrami-equation is:

$$\alpha_i = 1 - \exp\left(-a_i(t - b_i)^{c_i}\right) \tag{6}$$

where $t$ is the age of the sample (expressed in days), $a_i$, $b_i$, and $c_i$ are reaction constants (determined empirically by Taylor and reported by Jennings and Tennis [46]) and $\alpha_i$ is the degree of hydration of the $i$th reactant, defined as the ratio between the amount of phase $i$ reacted and the initial amount of phase $i$:

$$\alpha_i = \frac{[i]_0 - [i]_t}{[i]_0} \tag{7}$$

where $[i]_t$ is the amount of unreacted phase $i$ at time $t$.

The calculated composition is reported in Table 4 as grams per 100 g of fresh paste. In accordance with XRD findings, the only cement phase which survived after 14-month leaching is $C_2S$, while $C_3S$, $C_3A$ $C_4AF$ and gypsum fully reacted. Furthermore, in accordance with quantitative TGA findings, calculated amounts of carbonates are almost the same in the two series (A and B), even if slightly underestimated by the model, while portlandite was consumed slightly more in the B series than in the A one.

However, in order to compare the results of Rietveld analysis (Fig. 7) with those calculated from this hydration scheme, percentage phase composition values referred to the total crystalline fraction including only the phases modelled by the Rietveld algorithm are reported in Table 5. As far as portlandite is considered, the results from the model seem to agree quite well with those obtained by Rietveld analysis, in the other cases the agreement is less satisfactory. On average, the model underestimates carbonates while it is the opposite for $C_4A\underline{C}H_{11}$ and $C_2S$.

An elemental composition was calculated from the phase composition to be directly compared with the ESEM data. Fig. 8 shows the results for the B1 specimen concerning oxygen, calcium, silicon and sulphur (the most abundant elements): the match is good at high depth, but a substantial difference in the trends is evident near the surface.

The difference can be easily explained by directly comparing the diffraction patterns taken at increasing depths: the amorphous content seems to increase going from the interior to the surface (as the intensity of the amorphous bumps increases). This is expected as an effect of leaching; as

suggested by Faucon et al. [53] contact with a demineralised solution induces surface precipitation of short chain C-S-H which, of course, is amorphous in nature. An effective way of accounting for this is through the use of an error-function (erf)-like (function compatible with a diffusion process in a semi-infinite specimen) or exponential-like (very similar to the erf) gradient function. The parameters of the gradient function can be tuned as to give the expected amorphous content in the specimen core and to be effective just in the leached zone.

For instance, assuming that the amorphous quantity is $33.79+20\exp(-x/1000)$ where $x$ is the depth (in μm) measured from the surface inwards, the result of Fig. 9 can be obtained for the B1 specimen (analogous results were obtained for all other specimens investigated but for brevity they are not shown here).

The curves, plotted with an expanded ordinate axis for clarity, match within the errors of the EDXS and XRD quantitative data (few percent each). Large differences on the oxygen content are likely being water a source for this element. Calculated residual water content can in fact be different from the value measured via EDXS in the ESEM (working at low air pressure and not in vacuum) and is not taken into account by the Rietveld refinement (as water is not present as ice).

## 5. Conclusions

The addition of organoclay is highly effective in sequestering the model organic waste (2-CA) used in the present study, especially if compared with previous results where 2-CA was almost totally leached when it was directly admixed with the cementitious binder without any sorbent agent [33]. Indeed, the maximum amount of contaminant released after 14 months of leaching is 30% in the worst analysed case (25,000 ppm initial load). However, two samples, A1 and B1, had a very limited release (less than about 12%), also considering the prolonged DLT; in no other literature work investigating S/S processes of organic pollutants [15–24] the leaching tests, if performed, lasted so many months.

The organoclay amount plays an important role in the effectiveness of S/S; indeed, it strongly influences the open porosity and shifts the average pore radius towards the 50–70 nm range with a predominance of large and medium capillary pores, on which permeability mainly depends. Thus the counterintuitive effect of the organoclay, i.e. the larger the amount the higher the release, is accounted for by the porosity increase with its amount.

The influence of the 2-CA on hydration of cement pastes, clearly observed when directly admixed with the binder [33], is here highly mitigated by the presence of the organoclay which sequesters the contaminant from the pore solution. Indeed, the portlandite content in control samples and contaminated ones is almost the same after the 28-day curing.

Long-term leaching modifies the mineral composition of the monoliths: at a depth from the surface of the order of a few mm, a well-defined leaching boundary is observed. In this zone, a phase composition gradient has been identified and characterised: calcite is more abundant towards the exterior where, conversely, portlandite decreases.

EDXS, mainly Si profile (Fig. 8), and XRD (Fig. 7) results indicate that a large fraction of amorphous C-S-H is present in the near-surface region of the wasteform, decreasing towards the interior. The proposed exponential trend, seems to fit well the experimental EDXS data (Fig. 9).

## Acknowledgements

This work was supported by the basic research funds of the Italian Ministry of University and Research, PRIN 2003–2004 project “Mechanisms of surface interactions in mineral phases: kinetics of dissolution, of crystal growth and their modeling”.

## References

[1] R.D. Spence, C. Shi (Eds.), Stabilization and Solidification of Hazardous, Radioactive, and Mixed Wastes, CRC Press, Boca Raton, 2005.
[2] SpenceR.D. (Ed.), Chemistry and Microstructure of Solidified Waste Forms, Lewis Publishers, Boca Raton, 2000.
[3] O. Yilmaz, K. Ünlü, E. Cokca, Solidification/stabilization of hazardous wastes containing metals and organic contaminants, J. Environ. Eng. 129 (2003) 366–376.
[4] K. Brodersen, K. Nilsson, Pores and cracks in cemented waste and concrete, Cem. Concr. Res. 22 (1992) 405–417.
[5] C.D. Hills, S.J.T. Pollard, The influence of interference effects on the mechanical, microstructural and fixation characteristics of cement-solidified hazardous waste forms, J. Hazard Mater. 52 (1997) 171–191.
[6] C.S. Poon, Z.Q. Chen, O. Wai, A flow-through leaching model for monolithic chemically stabilized/solidified hazardous waste, J. Air Waste Manage. Assoc. 49 (1999) 569–575.
[7] P.L. Bishop, R. Gong, T.C. Keener, Effects of leaching on pore size distribution of solidified/stabilized wastes, J. Hazard Mater. 31 (1992) 59–74.
[8] L.C. Lange, C.D. Hills, A.B. Poole, Preliminary investigation into the effects of carbonation on cement-solidified hazardous wastes, Environ. Sci. Technol. 30 (1996) 25–30.
[9] J.C. Walton, S. Bin-Shafique, R.W. Smith, N. Gutierrez, A. Tarquin, Role of carbonation in transient leaching cementitious wasteforms, Environ. Sci. Technol. 31 (1997) 2345–2349.
[10] K.Y. Cheng, P. Bishop, J. Isenburg, Leaching boundary in cement-based waste forms, J. Hazard Mater. 30 (1992) 285–295.
[11] K.Y. Cheng, L.P. Bishop, Leaching boundary movement in solidified/stabilized waste forms, J. Air Waste Manage. Assoc. 42 (1992) 164–168.
[12] M.Z. Islam, L.J.J. Catalan, E.K. Yanful, A two-front leach model for cement-stabilized heavy metal waste, Environ. Sci. Technol. 38 (2004) 1522–1528.
[13] B. Batchelor, Leach models: theory and application, J. Hazard Mater. 24 (1990) 255–266.
[14] L. Tiruta-Barna, A. Imyim, R. Barna, Long-term prediction of the leaching behavior of pollutants from solidified wastes, Adv. Environ. Res. 8 (2004) 697–711.
[15] D.M. Montgomery, C.J. Sollars, T.S. Sheriff, R. Perry, Organophilic clays for the successful stabilisation/solidification of problematic industrial wastes, Environ. Technol. Lett. 9 (1988) 1403–1412.
[16] S. Paria, P.K. Yuet, Solidification–stabilization of organic and inorganic contaminants using Portland cement: a literature review, Environ. Rev. 14 (2006) 217–255.
[17] D.M. Montgomery, C.J. Sollars, R. Perry, S.E. Tarling, P. Barnes, E. Handerson, Treatment of organic-contaminated industrial wastes using cement-based stabilization/solidification — II. Microstructural analysis of the organophilic clay as a pre-solidification adsorbent, Waste Manage. Res. 9 (1991) 113–125.
[18] H.S. Shin, K.S. Jun, Cement-based stabilization solidification of organic contaminated hazardous wastes using Na-bentonite and silica-fume, J. Environ. Sci. Health., Part A — Toxic Hazard Substance Environ. Eng. 30 (1995) 651–668.

[19] I.M.-C. Lo, Solidification/stabilization of phenolic waste using organic-clay complex, J. Environ. Eng. 122 (1996) 850–855.
[20] R. Cioffi, L. Maffucci, L. Santoro, F.P. Glasser, Stabilization of chloro-organics using organophilic bentonite in a cement-blast furnace slag matrix, Waste Manage. 21 (2001) 651–660.
[21] G. Calvanese, R. Cioffi, L. Santoro, Cement stabilization of tannery sludge using quaternary ammonium salt exchanged bentonite as pre-solidification adsorbent, Environ. Technol. 23 (2002) 1051–1062.
[22] D. Botta, G. Dotelli, R. Biancardi, R. Pelosato, I. Natali Sora, Cement-clay pastes for stabilization/solidification of 2-chloroaniline, Waste Manage. 24 (2004) 207–216.
[23] P. Gong, P.L. Bishop, Evaluation of organics leaching from solidified/stabilized hazardous wastes using a powder reactivated carbon additive, Environ. Technol. 24 (2003) 445–455.
[24] V.M. Hebatpuria, H.A. Arafat, P.L. Bishop, N.G. Pinto, Leaching behavior of selected aromatics in cement-based solidification/stabilization under different leaching tests, Environ. Eng. Sci. 16 (1999) 451–463.
[25] E. Argese, C. Bettiol, F. Agnoli, A. Zambon, M. Mazzola, A. Volpi Ghirardini, Assessment of chloroaniline toxicity by the submitochondrial particle assay, Environ. Toxicol. Chem. 20 (2001) 826–832.
[26] Q. Zhou, F.P. Glasser, Thermal stability and decomposition mechanisms of ettringite at < 120° C, Cem. Concr. Res. 31 (2001) 1333–1339.
[27] UNICEN 8798, Radioactive Waste Solidification Products — Long Term Leach Test, UNI Ente Nazionale Italiano di Unificazione, Milano, Italy, December 1986 in Italian.
[28] M. Leoni, U. Welzel, P. Scardi, Polycapillary optics for materials science studies: instrumental effects and their correction, J. Res. Natl. Inst. Stand. Technol. 109 (2004) 27–48.
[29] U. Welzel, M. Leoni, Use of polycapillary X-ray lenses in the X-ray diffraction measurement of texture, J. Appl. Crystallogr. 35 (2002) 196–206.
[30] I. Natali Sora, R. Pelosato, L. Zamponi, D. Botta, G. Dotelli, M. Vitelli, Matrix optimisation for hazardous organic waste sorption, Appl. Clay Sci. 28 (2005) 43–54.
[31] H.F.W. Taylor, Cement Chemistry, 2nd Edition, Thomas Telford, London, 1997, p. 247.
[32] J.J. Thomas, H.M. Jennings, A.J. Allen, The surface area of hardened cement paste as measured by various techniques, Concr. Sci. Eng. 1 (1999) 45–64.
[33] I. Natali Sora, R. Pelosato, D. Botta, G. Dotelli, Chemistry and microstructure of cement pastes admixed with organic liquids, J. Eur. Ceram. Soc. 22 (2002) 1463–1473.
[34] H. Krøyer, H. Lindgreen, H.J. Jakobsen, J. Skibsted, Hydration of Portland cement in the presence of clay minerals studied by $^{29}Si$ and $^{27}Al$ MAS NMR spectroscopy, Adv. Cem. Res 15 (2003) 103–112.
[35] F.-J. Ulm, E. Lemarchand, F.H. Heukamp, Elements of chemomechanics of calcium leaching of cement-based materials at different scales, Eng. Fract. Mech. 70 (2003) 871–889.
[36] K.L. Scrivener, T. Füllmann, E. Gallucci, G. Walenta, E. Bermejo, Quantitative study of Portland cement hydration by X-ray diffraction/Rietveld analysis and independent methods, Cem. Concr. Res. 34 (2004) 1541–1547.
[37] K. Haga, M. Shibata, M. Hironaga, S. Tanaka, S. Nagasaki, Change in pore structure and composition of hardened cement paste during the process of dissolution, Cem. Concr. Res. 35 (2005) 943–950.
[38] I.M.-C. Lo, C.-I. Tang, X.-D. Li, C.-S. Poon, Leaching and microstructural analysis of cement-based solidified wastes, Environ. Sci. Technol. 34 (2000) 5038–5042.
[39] Y. Fu, P. Xie, P. Gu, J.J. Beaudoin, Effect of temperature on sulphate adsorption/desorption by tricalcium silicate hydrates, Cem. Concr. Res. 24 (1994) 1428–1432.
[40] R.A. Young, The Rietveld method, Oxford University Press, New York, 1995.
[41] L.B. McCusker, R.B. Von Dreele, D.E. Cox, D. Louër, P. Scardi, Rietveld refinement guidelines, J. Appl. Crystallogr. 32 (1999) 36–50.
[42] N.V.Y. Scarlett, I.C. Madsen, L.M.D. Cranswick, T. Lwin, E. Groleau, G. Stephenson, M. Aylmore, N. Agron-Olshina, Outcomes of the International Union of Crystallography Commission on Powder Diffraction Round Robin on Quantitative Phase Analysis: samples 2, 3, 4, synthetic bauxite, natural granodiorite and pharmaceuticals, J. Appl. Crystallogr. 35 (2002) 383–400.
[43] I.C. Madsen, N.V.Y. Scarlett, L.M.D. Cranswick, T. Lwin, Outcomes of the International Union of Crystallography Commission on Powder Diffraction Round Robin on Quantitative Phase Analysis: samples 1a to 1h, J. Appl. Crystallogr. 34 (2001) 409–426.
[44] D.P. Bentz, Three-dimensional computer simulation of Portland cement hydration and microstructure development, J. Am. Ceram. Soc. 80 (1997) 3–21.
[45] E.M. Gartner, J.F. Young, D.A. Damidot, I. Jawed, Hydration of Portland cement, in: J. Bensted, P. Barnes (Eds.), Structure and Performance of Cements, Second Edition, Spoon Press, London, 2002, pp. 84–88.
[46] H.M. Jennings, P.D. Tennis, Model for the developing microstructure in Portland cement pastes, J. Am. Ceram. Soc. 77 (1994) 3161–3172 Correction published in the J Am Cer Soc 78 (1995) 2575.
[47] V.G. Papadakis, Experimental investigation and theoretical modelling of silica fume activity in concrete, Cem. Concr. Res. 29 (1999) 79–86.
[48] H.J. Kuzel, H. Pollmann, Hydration of $C_3A$ in the presence of $Ca(OH)_2$, $CaSO_42H_2O$ and $CaCO_3$, Cem. Concr. Res. 21 (1991) 885.
[49] H.J. Kuzel, Initial hydration reactions and mechanisms of delayed-ettringite formation in Portland cements, Cem. Concr. Comp. 18 (1996) 195–203.
[50] D.P. Bentz, CEMHYD3D: A Three-Dimensional Cement Hydration and Microstructure Development Modeling Package, NIST, Gaithersburg, June 2005, p. 25, Version 3.0.
[51] F. Cella, T. Cerulli, A. Bravo, D. Salvioni, M. Squinzi, A. Lo Presti, M. Merlini, Influence of the $CO_2$ Dissolved in Pore Water on the Stability of Sulphoaluminate Hydrates: A Case History, Proceedings of the 27th International Conference on Cement Microscopy-April 24–28, ICMA, Victoria — Canada, 2005, CD-ROM.
[52] M. Fukuhara, S. Goto, K. Asaga, M. Daimon, R. Kondo, Mechanisms and kinetics of $C_4AF$ hydration with gypsum, Cem. Concr. Res. 11 (1981) 407–414.
[53] P. Faucon, F. Adenot, J.F. Jacquinot, J. Virlet, R. Cabrilac, M. Jorda, in: H. Justnes (Ed.), Contribution of Nuclear Magnetic Resonance Techniques to the Study of Cement Paste Water Degradation, Proceedings of the 10th International Congress on the Chemistry of Cement, vol. 3, 3v003, Göteborg, Sweden, 1997.